Independently tunable multichannel terahertz filters*

Zhang Hui-Yun(张会云), Gao Ying(高 营),
Zhang Yu-Ping(张玉萍)†, and Wang Shi-Fan(王世范)

College of Science, Shandong University of Science and Technology, Qingdao 266510, *China*

(Received 18 March 2011; revised manuscript received 19 April 2011)

We numerically demonstrate terahertz multichannel filters with independently tunable defect modes based on fractal photonic crystals. Single defect and multiple defects models are proposed to fabricate the multichannel terahertz filters. The facts that the wave functions of the defect states do not overlap and their bases are orthogonal lead to the independency among the defect modes. The simulated results theoretically provide the principle for fabricating independently tunable multichannel terahertz filters by utilizing one-dimensional photonic crystals with defects.

Keywords: fractal structure, photonic crystal, terahertz filter, defect

PACS: 41.20.Jb, 78.20.Ci, 87.50.U–, 43.58.Kr **DOI:** 10.1088/1674-1056/20/9/094101

1. Introduction

Terahertz (THz) waves ranging from 30 μm to 3 mm bridge the gap between the microwave and the infrared regions, and have attracted extensive attention during the past decades. Due to its potential applications in biological imaging and sensing,[1,2] nanotechnology,[3] security[4] and free space communication,[5] THz radiation is gradually playing a unique role in the relevant fields.

As an indispensable device for ultrafast information processing and the interconnection of terahertz wave communication, the terahertz wave filter has developed rapidly. In recent years, terahertz wave filters based on photonic crystals, metamaterial or surface plasmon have been reported. Nìmec *et al.*[6] demonstrated a high-quality smart filter based on photonics crystals (PCs) for the terahertz range. Its relative tunability reached 20% and the peak transmission of the tunable defect mode was about −6 dB at 0.35 THz. Chen and Meng[7] presented a new type of terahertz photonic crystal filter, which included the waveguide and the frequency selection parts. A terahertz modulator was proposed based on a one-dimensional (1D) photonic crystal,[8] in which the transmitted terahertz waves could be modulated by different carrier densities in the semiconductor controlled by the applied voltage. Brand *et al.*[9] and Gallant *et al.*[10] theoretically and experimentally demonstrated the use of photonic structures consisting of finite two-dimensional (2D) square arrays of metallic pillars to achieve the filtering of the radiation in the terahertz frequency region. Melo *et al.*[11] have fabricated filters based on metal mesh structures centred at frequencies ranging from 0.4 THz to 10 THz by using photolithography and electroforming techniques.

It is well known that photonic crystals provide a good base for the design of optical devices owing to their unique abilities to control and manipulate light.[12] The PCs and the defect modes in the PCs in the THz domain have been investigated for more than 20 years. Toshiaki *et al.*[13] fabricated a sample with a nonlinear optical material as the defect in a 1D PC structure and studied the nonlinear transmission of the sample experimentally with a nanosecond laser. 2D photonic crystals constructed with intrinsic semiconductor rods, which could be applied to the tunable filters operating at the THz range, were reported.[14] The position of the defect was studied experimentally as a function of the thickness of the defect layer and it was shown to behave in a donor mode.[15] Mounaix *et al.*[16] used a spin crossover material as the defect inserted into a periodic structure of alternating

*Project supported by the National Natural Science Fundation of China (Grant No. 61001018), the Research Fund of Shandong University of Science and Technology, China (Grant No. 2010KYJQ103), the Shandong University of Science and Technology Foundation, China (Grant No. YCA100428), and the Open-fund of Key Laboratory of Opto-electronic Information Science and Technology of Ministry of Education, China.

†Corresponding author. E-mail: zhangyuping1976@yahoo.com.cn

© 2011 Chinese Physical Society and IOP Publishing Ltd

layers of glass and air. They experimentally demonstrated that the defect level position was controlled by the dielectric hysteresis property of the spin crossover materials. Yee and Mark[17] experimentally showed a single sharp resonance near 1 THz with a quality factor Q as high as 1020 by using photonic crystal cavities. Rajind *et al.*[18] experimentally and theoretically demonstrated a tunable universal terahertz filter using artificial dielectrics based on parallel-plate waveguides. One-dimensional photonic crystal structures for the multiple-channel and the polarization selective filterings in the terahertz range were studied theoretically.[19] In the experiment by Yuan *et al.*,[20] the width of the air defect layer was changed by a piezoelectric actuator. By breaking the periodicity of the photonic crystal, it is possible to create highly localized defect modes within the photonic band-gap, which are similar to the localized impurity states in a semiconductor.[21] However, only a few papers dealt with the tunability of the defect modes.[22,23] In the present study, we report tunable THz filters based on one-dimensional PCs with defects and numerically demonstrate that the structure can not only produce some defect modes but can also be tuned separately for their numbers, corresponding frequencies and frequency intervals.

2. Computational model and numerical method

We consider a 1D PC comprised of identical alternating layers of high ($n_{\rm H}$) and low ($n_{\rm L}$) refractive indices, with their optical thicknesses $T_{\rm H} = n_{\rm H}d_{\rm H} = \lambda_0/4$ and $T_{\rm L} = n_{\rm L}d_{\rm L} = \lambda_0/4$, where $d_{\rm H}$ and $d_{\rm L}$ are the physical thicknesses of the two layers. When the electrical or the optical thickness of each layer is equal to one-quarter wavelength at a particular frequency, the maximum reflection is obtained, since all voltage standing wave ratios (VSWRs) multiply at this frequency to give the input VSWR.[24] Zirconium oxide ($n_{\rm H} = 2.1$) and magnesium fluoride ($n_{\rm L} = 1.4$) are selected as the high-index and the low-index materials, respectively, because their absorptions[25] in the THz band are 0.3 cm^{-1} and 0.0001 cm^{-1}, respectively. Terahertz frequencies can be used in terahertz wave wireless communication. Therefore, the design wavelength in this paper is selected to be $\lambda_0 = 1$ mm, corresponding to the frequency of 0.3 THz within the less atmospheric loss window.

In order to overcome the shortcoming that the defect modes of the PCs are interactive and cannot be tuned independently, fractal 1D PCs with a single defect layer or multiple defect layers are presented in this paper. The construction procedure of the 1D fractal photonic structure is based on the method of coupling defect layers. We begin with a periodic multilayer initiator S_0 of $(\rm HL)^m$ or $(\rm LH)^m$, where H and L represent the layers of high ($n_{\rm H}$) and low ($n_{\rm L}$) refractive indices with optical thicknesses $T_{\rm H}$ and $T_{\rm L}$, respectively, and m is the number of the periods. Then, by coupling a defect layer between the initiators $(\rm HL)^m$ and $(\rm LH)^m$, the first stage of the fractal $S_1 = (\rm HL)^m D_1 (\rm LH)^m$ is formed. Next, when another defect layer is inserted between two S_1, the second stage of the fractal S_2 is formed. Here, we propose photonic crystal structure models with wedge-shape defect layers, as shown in Fig. 1. We can see that the thickness of defect layer D_2 increases (see Fig. 1(a)) and the thicknesses of both D_1 defect layers increase as the vertical incident position goes down (see Fig. 1(b)). So we can change the thicknesses of the defect layers independently by changing the vertical position of the incident terahertz wave.

It is possible to obtain a self-similar fractal structure by repeating the given operation. The lower order fractal sequences are given as follows.

The multichannel single defect sequences are

$$\begin{aligned} S_0 &= (\rm HL)^m, \\ S_1 &= (\rm HL)^m D_1 (\rm LH)^m, \\ S_2 &= (\rm HL)^m D_1 (\rm LH)^m D_2 (\rm HL)^m D_1 (\rm LH)^m, \\ S_3 &= (\rm HL)^m D_1 (\rm LH)^m D_2 (\rm HL)^m D_1 (\rm LH)^m D_3 \\ &\quad (\rm HL)^m D_1 (\rm LH)^m D_2 (\rm HL)^m D_1 (\rm LH)^m, \\ &\quad \cdots, \end{aligned}$$

where D_1, D_2, D_3, ... are the defect layers with thicknesses of $d_1 = \alpha d_{\rm H}$, $d_2 = \beta d_{\rm L}$, $d_3 = \gamma d_{\rm L}$, ..., respectively. The α, β, and γ are constants. The corresponding refractive indices are $n_1 = n_{\rm H}$, $n_2 = n_3 = n_{\rm L}$, ... i.e., the optical thicknesses of D_1, D_2, D_3, ... are $\alpha T_{\rm H}$, $\beta T_{\rm L}$, $\gamma T_{\rm L}$, ...

The multichannel multidefect sequences are

$$\begin{aligned} S_0 &= (\rm HL)^m, \\ S_1 &= (\rm HL)^m D_1 (\rm LH)^m D_1, \\ S_2 &= [(\rm HL)^m D_1 (\rm LH)^m D_2]^2, \\ S_3 &= [(\rm HL)^m D_1 (\rm LH)^m D_2 (\rm HL)^m D_1 (\rm LH)^m D_3]^2, \\ &\quad \cdots. \end{aligned}$$

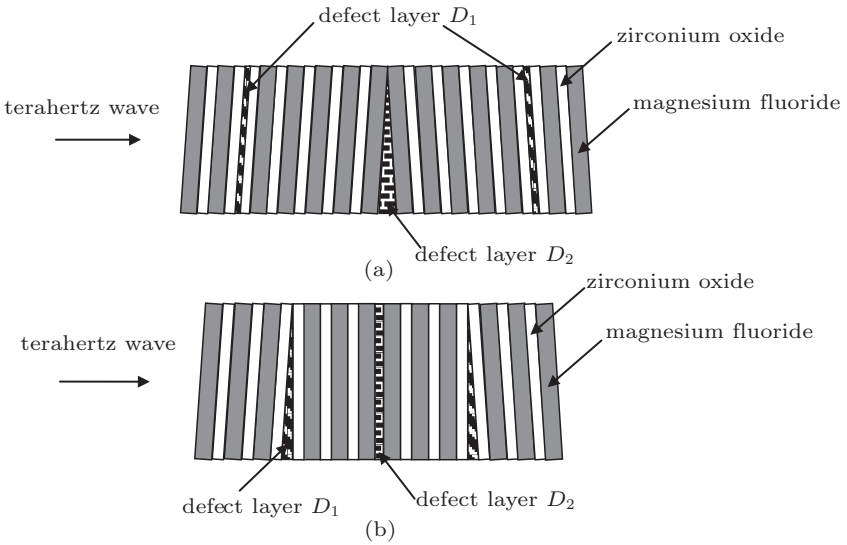


Fig. 1. Schematic diagrams of photonic crystals with wedge-shape defect layers. (a) D_2 is wedge-shape defect layer. (b) D_1 is wedge-shape defect layer.

Depending on different circumstances, D_1, D_2, D_3, ... can be defined separately. To fabricate the double-defect sequence, we select

$$D_1 = \alpha \mathrm{H}(\mathrm{LH})^n \mathrm{L}\alpha\mathrm{H}, \quad D_2 = \beta L(\mathrm{HL})^l \mathrm{H}\beta\mathrm{L},$$
$$D_3 = \gamma \mathrm{L}(\mathrm{HL})^p \mathrm{H}\gamma\mathrm{L}, \ldots .$$

For the triple-defect sequence, we choose

$$\begin{aligned} D_1 &= \alpha \mathrm{H}(\mathrm{LH})^n \mathrm{L}\alpha\mathrm{H}(\mathrm{LH})^n \mathrm{L}\alpha\mathrm{H}, \\ D_2 &= \beta \mathrm{L}(\mathrm{HL})^l \mathrm{H}\beta\mathrm{L}(\mathrm{HL})^l \mathrm{H}\beta\mathrm{L}, \\ D_3 &= \gamma \mathrm{L}(\mathrm{HL})^p \mathrm{H}\gamma\mathrm{L}(\mathrm{HL})^p \mathrm{H}\gamma\mathrm{L}, \\ &\cdots . \end{aligned}$$

The transmittances of the above structures can be obtained by using the transfer-matrix method. Let a wave be incident at an angle θ from the vacuum into the fractal structure. Suppose that the wave in the l-th layer has a wave vector $\boldsymbol{k}_l = k_{lx}\boldsymbol{x} + k_{lz}\boldsymbol{z}$, whose magnitude is $\omega n_l/c$, where c is the speed of light in the vacuum and n_l is the l-th layer refractive index. The amplitudes of the electric components of the forward and the backward waves can be related via a transfer matrix

$$\boldsymbol{M}_l = \begin{pmatrix} \cos k_{lz} d_l & \mathrm{i} \sin k_{lz} d_l / \eta_l \\ \mathrm{i}\eta_l \sin k_{lz} d_l & \cos k_{lz} d_l \end{pmatrix}, \qquad (1)$$

where $\eta_l = n_l \sqrt{1 - \sin^2 \theta_l \times n_{l-1}^2}$ for the transverse electric (TE) wave, θ_l is the incident angle and k_{lz} is the z component of wave vector k_l in the l-th layer. Thus the total transfer matrix can be obtained by multiplying all individual transfer matrices in sequence. It can be calculated from

$$\boldsymbol{M} = \boldsymbol{M}_1 \boldsymbol{M}_2 \boldsymbol{M}_3 \ldots \boldsymbol{M}_N = \begin{pmatrix} x_{11} & x_{12} \\ x_{21} & x_{22} \end{pmatrix}. \qquad (2)$$

Similarly, the reflection response and the transmission coefficient will satisfy the recursions

$$\begin{cases} r = \dfrac{x_{12} q_0^2 + (x_{22} - x_{11})\, q_0 - x_{21}}{x_{12} q_0^2 + (x_{11} + x_{22})\, q_0 + x_{21}}, \\ t = \dfrac{2 q_0}{x_{12} q_0^2 + (x_{11} + x_{22})\, q_0 + x_{21}}, \end{cases} \qquad (3)$$

where $q_0 = \sqrt{\varepsilon_0}/\sqrt{\mu_0}\cos(\theta_0)$, θ_0 is the incident angle in vacuum, ε_0 and μ_0 are the permittivity and the permeability in vacuum, respectively. Thus, the total transmittance can be obtained as $T = t \cdot t^*$.

3. Simulation results

Here, we employ structure $S_1 = (\mathrm{HL})^m D_1 (\mathrm{LH})^m$ to design a bandpass filter with a single channel in the terahertz range. We can see that the fractal structure is self-symmetrical with a periodic structure S_0 and acts as an initiator. Figure 2 shows the transmittance of the fractal structure $S_1 = (\mathrm{HL})^6 D_1 (\mathrm{LH})^6$ at normal incidence. As shown in Figs. 2(a)–2(c), the frequency of the defect mode depends on the thickness of D_1 and α determines the optical thickness of the defect. When α changes from 1.7 to 2.0 and to 2.3, the location of the defect mode shifts to the left step by step. We define $\rho = 0.002$ THz as the filter tuning accuracy. In the process of tuning, if the full width at

half maximum (FWHM) of the defect mode is greater than ρ, we consider it to be beyond the tuning range. In this way, the tuning range of defect mode α is approximately 1.65–2.1 THz.

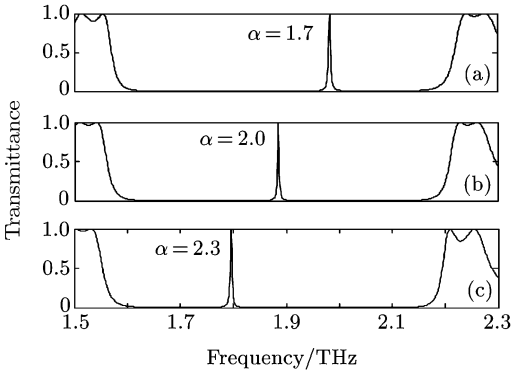


Fig. 2. Transmission spectra for $S_1 = (\mathrm{HL})^m D_1 (\mathrm{LH})^m$ with different coefficients α: (a) 1.7, (b) 2.0, (c) 2.3. The thickness of $\mathrm{D_1}$ is αT_{H} and $m = 6$.

Next, based on structure

$$S_2 = (\mathrm{HL})^m D_1 (\mathrm{LH})^m D_2 (\mathrm{HL})^m D_1 (\mathrm{LH})^m,$$

we insert a second defect, D_2. As shown in Fig. 3, there are two defect modes, which can be tuned independently. In Figs. 3(a)–3(c), we fix β at 0.5β and reduce α from 2.3 to 2.0 and to 1.7. It can be seen that defect mode β remains nearly invariant, while defect mode α shifts from 1.8007 THz to 1.8848 THz and then to 1.9824 THz. Similarly, defect mode α is steady, while defect mode β shifts from 1.9824 THz to 1.7562 THz and then to 1.8350 THz, if α is kept unvaried and β is changed from 0.5 to 0.3 and then to 0.1, as shown in Figs. 3(c)–3(e). Based on the numerical calculation, the tuning range of defect mode β is between 1.60 THz and 1.80 THz, and that of defect mode α is between 1.67 THz and 2.05 THz. The frequencies of defect modes α or β can be tuned independently in a certain range without affecting each other. It means that the interaction between the two defect modes of the proposed structure is avoided. To show how the defect modes are generated in the gap case, the electric field distributions inside the fractal structures corresponding to the two defect modes in Fig. 3(a) are investigated at frequencies of defect modes α and β, as shown in Fig. 4. The frequencies of the incident waves are 1.79575 THz and 1.68805 THz, respectively. It can be seen in Fig. 4(a) that the electric field corresponding to defect mode α is strongly localized in both defect layers D_1 but not in defect layer D_2. However, the electric field corresponding to defect mode β is mainly localized in D_2 instead of D_1, as shown in Fig. 4(b). Therefore, the coupling layers of D_1 and D_2 are two different kinds of defects and respectively relate to the corresponding defect states. The facts that the wave functions of the two kinds of defect states do not overlap and their bases are orthogonal leads to the independency between the two defect modes.

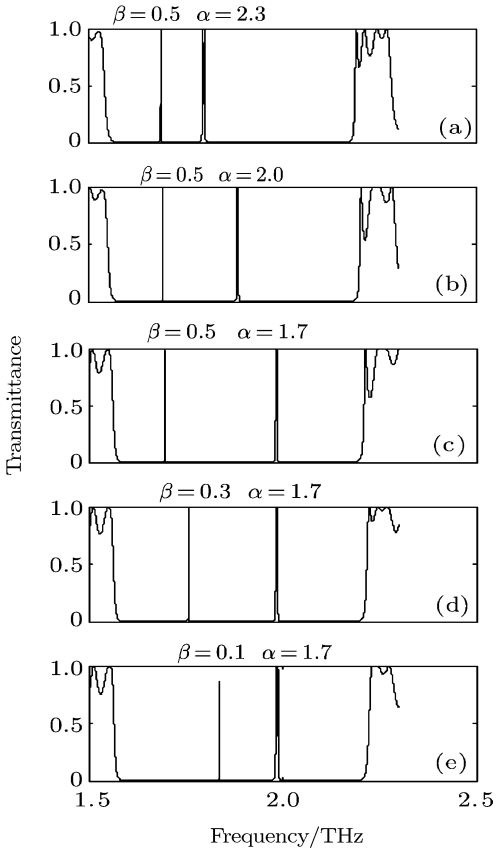


Fig. 3. Transmission spectra for structure $S_2 = (\mathrm{HL})^m D_1 (\mathrm{LH})^m D_2 (\mathrm{HL})^m D_1 (\mathrm{LH})^m$. The $\beta = 0.5$, α changes from 2.3 to 2.0 and then to 1.7 in panels (a)–(c) . The $\alpha = 1.7$, β changes from 0.5 to 0.3 to 0.1 in panels (c)–(e). The $D_1 = \alpha\mathrm{H}$, $D_2 = \beta\mathrm{L}$ and $m = 6$.

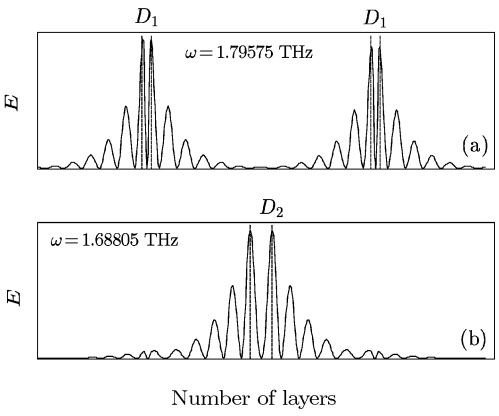


Fig. 4. Electric field distributions corresponding to the two defect modes in Fig. 3(a). The areas between the dashed lines correspond to D_1 and D_2 defect layers.

We can acquire the third defect mode γ when defect layer D_3 is introduced. The above-mentioned properties still appear. When α and γ are fixed, β shifts from 0.7 to 0.5 and then to 0.3, defect modes α and γ remain nearly invariant, defect mode β shifts from 1.6518 THz to 1.6955 THz and then to 1.7562 THz, as shown in Figs. 5(a)–5(c). In the same way, if we change the third coefficient and keep the other two coefficients unchanged, a similar result will emerge, as shown in Figs. 5(c)–5(e). It can be seen that all of the three defect modes can be tuned separately. If defect mode γ needs to be moved to a definite frequency while keeping defect modes α and β fixed, we just need to adjust the structural parameters of D_3 to meet the requirement. The same is true

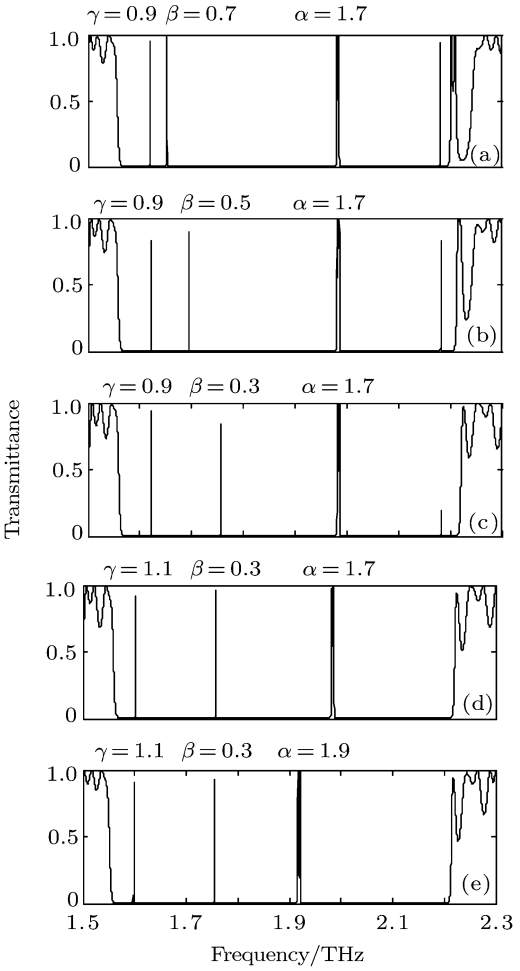


Fig. 5. Transmission spectra for structure $S_3 = (\mathrm{HL})^m D_1(\mathrm{LH})^m D_2(\mathrm{HL})^m D_1(\mathrm{LH})^m D_3(\mathrm{HL})^m D_1(\mathrm{LH})^m D_2(\mathrm{HL})^m D_1(\mathrm{LH})^m$ with different α, β and γ. In panels (a)–(c), α and γ are fixed, β shifts from 0.7 to 0.5 and then to 0.3. In panels (d)–(e), β and γ are fixed, α shifts from 1.7 to 1.9.

for defect modes α and β. Based on the numerical calculation, the tuning ranges of defect modes α, β and γ are about 1.77–2.07 THz, 1.64–01.77 THz and 1.57–1.64 THz, respectively.

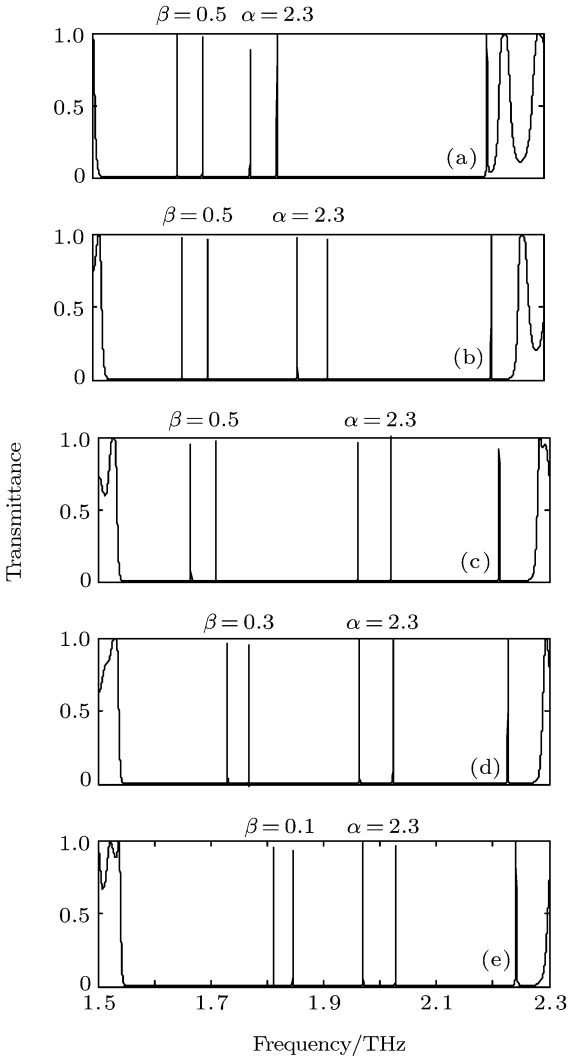


Fig. 6. Transmission spectra for structure $S_2 = [(\mathrm{HL})^m D_1(\mathrm{LH})^m D_2]^2$ with $D_1 = \alpha\mathrm{H}(\mathrm{LH})^n\mathrm{L}\alpha\mathrm{H}$, $D_2 = \beta L(\mathrm{HL})^l\mathrm{H}\beta\mathrm{L}$, $m = n = 4$, and $l = 6$. In panels (a)–(c), β is fixed, α shifts from 2.3 to 2.0 and then to 1.7. In panels (d) and (e), α is fixed, β shifts from 0.3 to 0.1.

Next, we establish four defect modes α_1, α_2, β_1 and β_2 using structure $S_2 = [(\mathrm{HL})^m D_1(\mathrm{LH})^m D_2]^2$. The results are shown in Fig. 6. Obviously, the relative positions of defect modes β_1 and β_2 will not change if coefficient α shifts with β unchanged, as shown in Figs. 6(a)–6(c). It means that defect modes β_1 and β_2 rely on coefficient β, while modes α_1 and α_2 depend on the value of α. Figures 6(c)–6(e) show the case in which β decreases and α remains unchanged. Moreover, we have investigated the dependences of defect modes α_i and β_i on period numbers n and l of D_1 and D_2, as shown in Fig. 7. It can be seen from Figs. 7(a)–7(c) that the frequency interval between modes α_1 and α_2 will narrow down if we increase n from 4 to 6 and

keep l a constant. The frequency interval between modes β_1 and β_2 will broaden as l decreases, and n is fixed, as shown in Figs. 7(c)–7(e). So the frequency intervals of the defect modes corresponding to different kinds of defects (D_1 or D_2) can also be tuned independently.

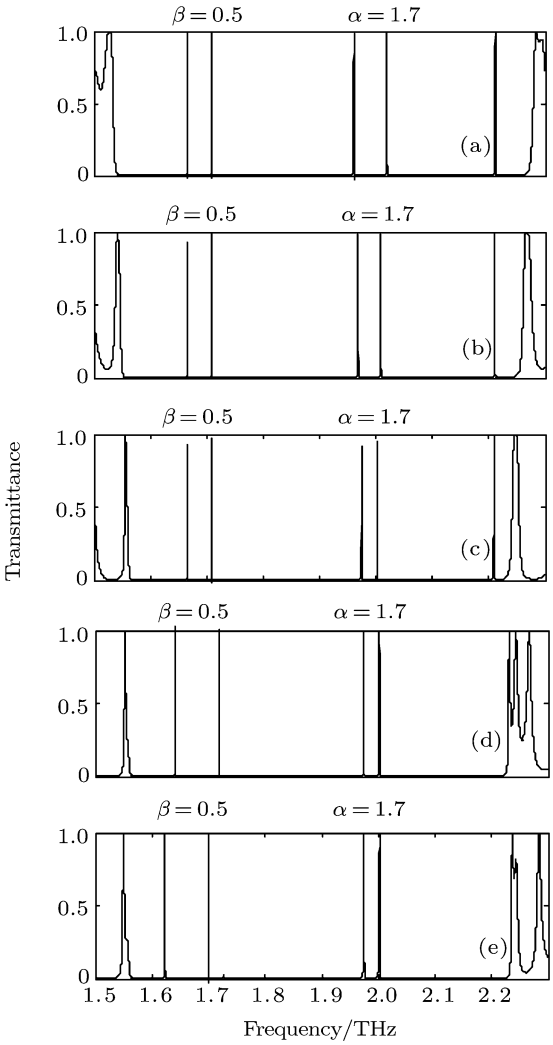


Fig. 7. Transmission spectra for structure $S_2 = [(\mathrm{HL})^m D_1 (\mathrm{LH})^m D_2]^2$ with $D_1 = \alpha\mathrm{H}(\mathrm{LH})^n\mathrm{L}\alpha\mathrm{H}$, $D_2 = \beta L(\mathrm{HL})^l\mathrm{H}\beta\mathrm{L}$, $\alpha = 1.7$, and $\beta = 0.5$. The period numbers are (a) $n = 4$ and $l = 6$, (b) $n = 5$ and $l = 6$, (c) $n = 6$ and $l = 6$, (d) $n = 6$ and $l = 4$, and (e) $n = 6$ and $l = 3$.

Similarly, we employ structure $S_2 = [(\mathrm{HL})^m D_1 (\mathrm{LH})^m D_2]^2$ in the simulation below. Let D_1 equal $\alpha\mathrm{H}(\mathrm{LH})^n\mathrm{L}\alpha\mathrm{H}(\mathrm{LH})^n\mathrm{L}\alpha H$ and D_2 equal $\beta\mathrm{L}(\mathrm{HL})^l\mathrm{H}\beta\mathrm{L}(\mathrm{HL})^l\mathrm{H}\beta\mathrm{L}$, we can obtain six defect modes α_1, α_2, α_3, β_1, β_2 and β_3, as shown in Fig. 8. When we shift the value of β from 0.5 to 0.4 and then to 0.3 while keeping α at a constant of 1.7, defect modes β_1, β_2 and β_3 change, and defect states α_1, α_2 and α_3 are invariant, as shown in Figs. 8(a)–8(c). By exchanging the variable and the invariable quantities, a similar evolution will appear, as shown in Figs. 8(c)–8(e).

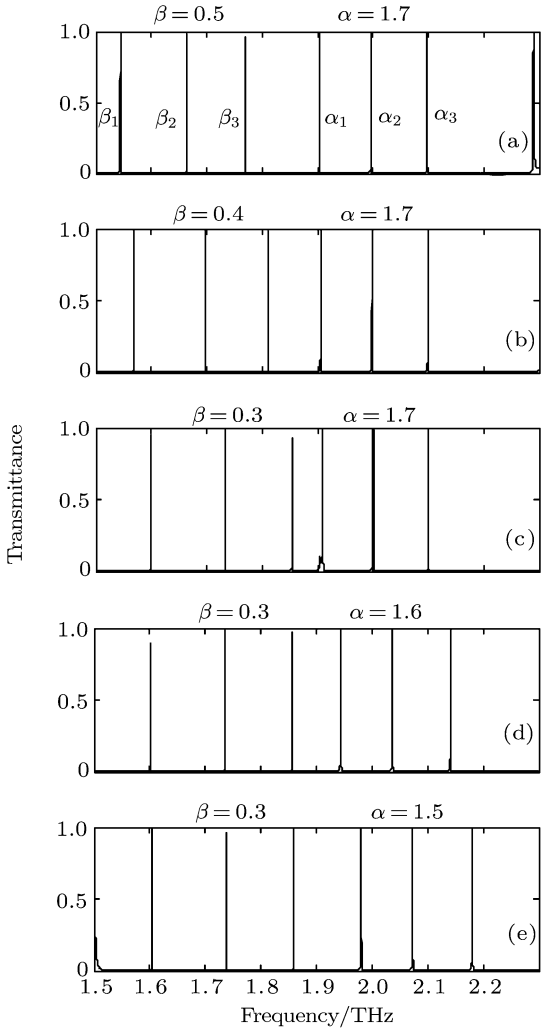


Fig. 8. Transmission spectra for structure $S_2 = [(\mathrm{HL})^m D_1 (\mathrm{LH})^m D_2]^2$ with $D_1 = \alpha\mathrm{H}(\mathrm{LH})^n\mathrm{L}\alpha\mathrm{H}(\mathrm{LH})^n\mathrm{L}\alpha\mathrm{H}$, $D_2 = \beta\mathrm{L}(\mathrm{HL})^l\mathrm{H}\beta\mathrm{L}(\mathrm{HL})^l\mathrm{H}\beta\mathrm{L}$, $m = 4$, and $n = l = 2$.

Finally, we discuss the tolerance of error for the defect modes. Figure 9 shows the modification of the defect mode in Fig. 2(b) when the incident angle has a 4% manufacturing tolerance. We can see that the tiny error of the incident angle does not affect the frequency of mode α at all, so we can use the structure shown in Fig. 1 to independently modify the thicknesses of the defect layers by changing the vertical position of the incident terahertz wave. As shown in Fig. 10, all the layers of the PCs including the defect layers have a 2% error in thickness. The shift of the defect mode is very clear. If the error only involves the defect layers, the variation range of the frequency for the defect mode is smaller than that in the case where each layer of the PCs has an error, as shown in

Fig. 11.

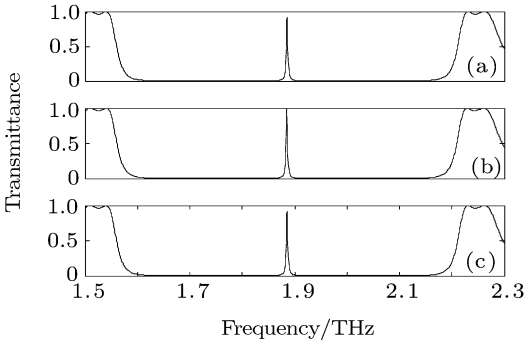


Fig. 9. Transmission spectra for $S_1 = (\mathrm{HL})^m D_1 (\mathrm{LH})^m$ with a 4% error in incident angle θ. The $\alpha = 2.0$ and $m = 6$. (a) $\delta\theta = +4\%$, (b) $\delta\theta = 0$, and (c) $\delta\theta = -4\%$.

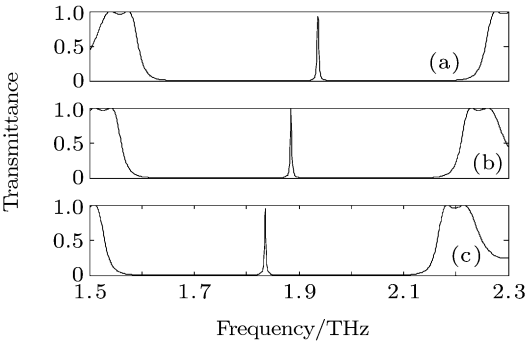


Fig. 10. Transmission spectra for $S_1 = (\mathrm{HL})^m D_1 (\mathrm{LH})^m$ with a 2% error in thicknesses d for all layers of the PCs, with $D_1 = \alpha\mathrm{H}$, $\alpha = 2.0$, and $m = 6$. (a) $\delta d = -2\%$, (b) $\delta d = 0$, and (c) $\delta d = +2\%$.

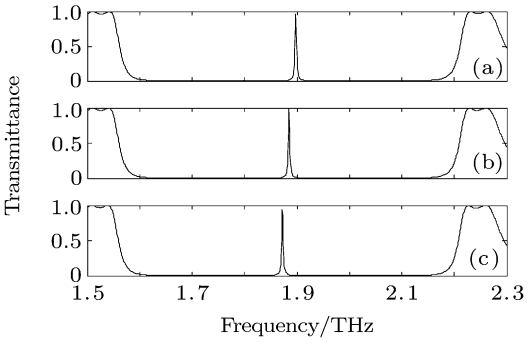


Fig. 11. Transmission spectra for $S_1 = (\mathrm{HL})^m D_1 (\mathrm{LH})^m$ with a 2% error in thicknesses D for the defect layers only, with $D_1 = \alpha\mathrm{H}$, $\alpha = 2.0$ and $m = 6$. (a) $\delta D = -2\%$, (b) $\delta D = 0$, and (c) $\delta D = +2\%$.

4. Conclusion

Fractal structure models based on one-dimensional photonic crystals are constructed to generate multiple defect modes for use at terahertz frequencies. The frequency, the frequency interval and the number of defect modes can be tuned separately by adjusting the structural parameters of the defect layers. By introducing errors, we provide the stability analysis. The conclusion is that the frequencies of these defect modes are insensitive to the error in the incident angle but are sensitive to the error in thickness.

References

[1] Xu J Z and Zhang X C 2006 *Appl. Phys. Lett.* **88** 151107
[2] Zhong H, Sanchez A R and Zhang X C 2006 *Opt. Express* **14** 9130
[3] Dragomana D and Dragoman M 2004 *Prog. Quant. Electron* **28** 66
[4] Federici J F, Schulkin B, Huang F, Gary D, Barat R, Oliveira F and Zimdars D 2005 *Semicond. Sci. Technol.* **20** 266
[5] Grant P D and Laframboise S R 2009 *Elctron. Lett.* **45** 18
[6] Nìmec H, Duvillaret L and Garet F 2004 *J. Appl. Phys.* **96** 8
[7] Chen H M and Meng Q 2011 *Acta Phys. Sin.* **60** 014202 (in Chinese)
[8] Zhang R and Cao J C 2010 *Acta Phys. Sin.* **59** 3924 (in Chinese)
[9] Brand S, Abram R A and Kaliteevski M A 2007 *Phys. Rev.* B **75** 035102
[10] Gallant A J, Kaliteevski M A, Brand S, Wood D, Petty M, Abram R A and Chamberlain J M 2007 *J. Appl. Phys.* **102** 023102
[11] Melo A M, Kornberg M A and Kaufmann P 2008 *Appl. Opt.* **47** 6064
[12] Joannopoulos J D 2008 *Photonic Crystals: Molding the Flow of Light* (New York: Biswas Hope Press)
[13] Hattori T, Tsurumachi N, Muroi N, Nakatsuka H and Ogino E 1996 *Prog. Cryst. Growth Charact.* **33** 183
[14] Kee C S and Lim H 2001 *Phys. Rev.* B **64** 121103
[15] Wostyn K, Zhao Y, de Schaetzen G, Hellemans L, Matsuda N, Clays K and Persoons A 2003 *Langmuir* **10** 19
[16] Mounaix P, Nguema E, Freysz E, Létard J F, Vigneras V and Calais O L 2007 *The 15th International Conference on Terahertz Electronics,* September 2–7, 2007, Cardiff, UK, p. 970
[17] Yee C M and Mark S S 2009 *Appl. Phys. Lett.* **94** 154104
[18] Rajind M, Abhishek N, Frank C and Daniel M M 2010 *Appl. Phys. Lett.* **97** 131106
[19] Zhao X X, Zhu Q F and Zhang Y 2009 *Chin. Phys.* B **18** 2864 (in Chinese)
[20] Yuan Z H, Wang M and Zhang J 2009 *Acta Sin. Quantum Optica* **15** 260
[21] Mehmet B, Temelkuran B and Ozbay E 2000 *Appl. Phys. Lett.* **77** 24
[22] Chelnokov A, Rowson S and Lourtioz J M 1998 *Electron. Lett.* 34 1965
[23] Nìmec H, Kužel P, Garet F and Duvillaret L 2005 *Opt. Lett.* **30** 549
[24] Young L and Cristal E G 1966 *IEEE Trans. Microwave Theory Tech.* **14** 75
[25] Li J S 2010 *Opt. Commun.* **283** 2647